The Arctic Frontal Zone as Seen in the NCEP–NCAR Reanalysis

MARK C. SERREZE, AMANDA H. LYNCH, AND MARTYN P. CLARK

Cooperative Institute for Research in Environmental Sciences, University of Colorado, Boulder, Colorado

(Manuscript received 11 February 2000, in final form 23 June 2000)

ABSTRACT

Calculations of a thermal front parameter using NCEP–NCAR reanalysis data over the period 1979–98 reveal a relative maximum in frontal frequencies during summer along northern Eurasia from about 60° to 70°N, best expressed over the eastern half of the continent. A similar relative maximum is found over Alaska, which is present year-round although best expressed in summer. These high-latitude features can be clearly distinguished from the polar frontal zone in the midlatitudes of the Pacific basin and collectively resemble the summertime ''Arctic frontal zone'' discussed in several early studies. While some separation between high- and midlatitude frontal activity is observed in all seasons, the summer season is distinguished by the development of an attendant mean baroclinic zone aligned roughly along the Arctic Ocean coastline and associated wind maxima in the upper troposphere. The regions of maximum summer frontal frequency correspond to preferred areas of cyclogenesis and to where the summertime contribution to annual precipitation is most dominant. Cyclones generated in association with the Eurasian frontal zone often track into the central Arctic Ocean, where they may have an impact on the sea-ice circulation. Development of the summertime Eurasian frontal zone and the summertime strengthening of the Alaskan feature appear to be largely driven by differential heating between the cold Arctic Ocean and warm snow-free land. Frontal activity also shows an association with orography. Several studies have argued that the location of the summer Arctic frontal zone may be in part determined by discontinuities in energy exchange along the tundra–boreal forest boundary. While such a linkage is not discounted here, a vegetation forcing is not required in this conceptual model.

1. Introduction

The concept of a region of frequent mesoscale frontal activity in northern high latitudes emerging as distinct from frontal activity in middle latitudes can be traced back to the early work of Dzerdzeevskii (1945). This high-latitude geographic feature was subsequently studied by Reed and Kunkel (1960), which using their terminology, is hereafter referred to as the ''Arctic frontal zone.'' Their study, based on fronts plotted on sumner (June–August) sea level pressure (SLP) analyses for the period 1952–56 (Fig. 1) revealed a belt of high frontal frequencies extending along the northern shores of Siberia and Alaska and southeastward across Canada. They argued that low frontal frequencies over Kamchatka and the high frequencies off Japan ''make it abundantly clear that the polar front remains separate from, and well to the south of, the Arctic frontal zone'' (Reed and Kunkel 1960, p. 496). The Arctic frontal zone was considered to exist in summer only, a view supported by a corresponding analysis of winter frontal frequencies, which failed to show a separate high-latitude feature. Reed and Kunkel further pointed out that the summer Arctic frontal zone merges with and can be viewed as an extension of the midlatitude polar frontal zone over Europe. Dzerdzeevskii (1945) also considered the Arctic frontal zone as a summer feature, and suggested that it arises from differential heating between the snow-free land surface and the cold Arctic Ocean. Reed and Kunkel (1960) countered that in view of large variations in the behavior of the frontal zone, additional factors, such as orography, must also be involved.

Conceptual models of the general circulation presented in early studies such as those by Palmén (1951), Defant and Taba (1957), and Palmén and Newton (1969) did not include a separate high-latitude feature that would correspond to the Arctic frontal zone. However, early Canadian analysis schemes (Anderson et al. 1955; Penner 1955) adopted a three-front model of the westerlies, with the northernmost representing individual ''Arctic fronts.'' The Meteorological Branch of Canada prepared routine synoptic charts showing the location of three fronts on the 850-, 700-, and 500-hPa levels. Differentiation between air masses and designation of fronts was based on wet-bulb temperature, vertical wind shear, and tropopause height. Using these data and hence presupposing Arctic fronts as present in any season, Barry (1967) examined the location of the Arctic frontal

Corresponding author address: Dr. Mark C. Serreze, CIRES, University of Colorado, Campus Box 449, Boulder, CO 80309.
E-mail: serreze@kyros.colorado.edu

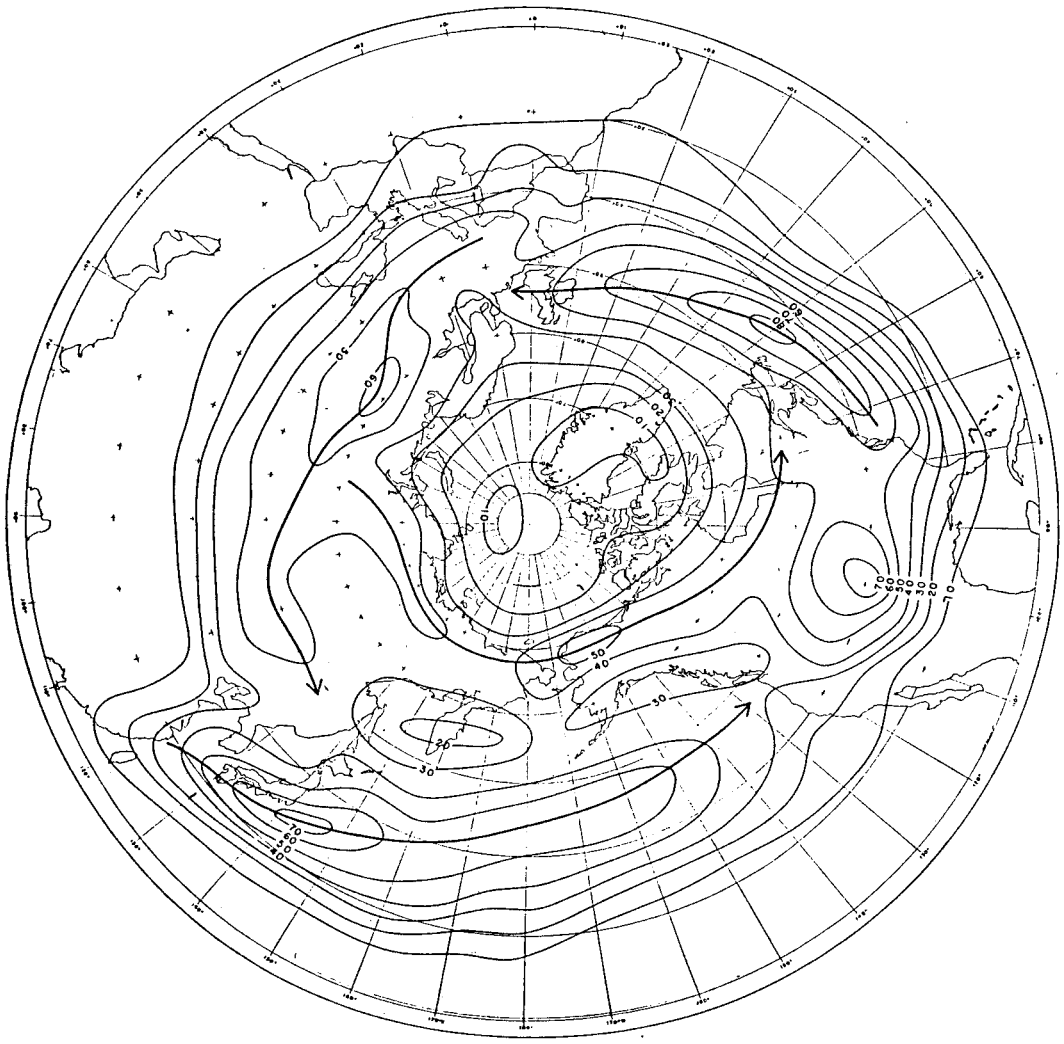

FIG. 1. Reed and Kunkel's (1960) map of the frequency of fronts in squares of 400 000 km^2 from Jun–Aug, based on SLP analyses for 1952–56. The heavy lines denote axes of maximum frontal frequency.

zone over North America for January, April, July, and October.

Based on a trajectory analysis of air masses for July, Bryson (1966) demonstrated that the modal position of the summer Arctic frontal zone over North America coincides closely with Reed and Kunkel's (1960) analysis as well as the position of the tree line. He postulated that the summer frontal position might be important in determining the distribution of forest versus tundra. However, Bryson also considered the frontal zone to exist during winter, aligned roughly along the southern margin of the boreal forest.

Hare (1968) and Hare and Ritchie (1972) offered the alternative hypothesis that the tundra/forest boundary may actually help to control the position of the frontal zone in summer due to contrasts in albedo, evaporation, and aerodynamic roughness. Pielke and Vidale (1996) elaborated on this concept. Drawing on findings from the Boreal Ecosystem Atmosphere Study (BOREAS), they suggested that stronger heating of the boreal forest from its lower albedo is not compensated by an increase in transpiration, even with the larger leaf area index of the forest. The heterogeneity (''patchiness'') of the boreal forest landscape gives rise to mesoscale circulations that help to mix the heat upward, giving rise to a deep thermal contrast between forest and tundra. In a parallel study, Pielke et al. (1996) showed evidence for linkage between frontal positions and the northern edge of the boreal forest over Canada based on data from the Canadian Regional Finite Element Model for May–September 1994. While the role of vegetation boundaries remains to be fully tested, a significant role of vegetation on regional and circumpolar climates on a range of timescales finds support in other studies (e.g., Bonan et al. 1992, 1995; Foley et al. 1994; Lynch et al. 1999).

Krebs and Barry (1970) subsequently examined what

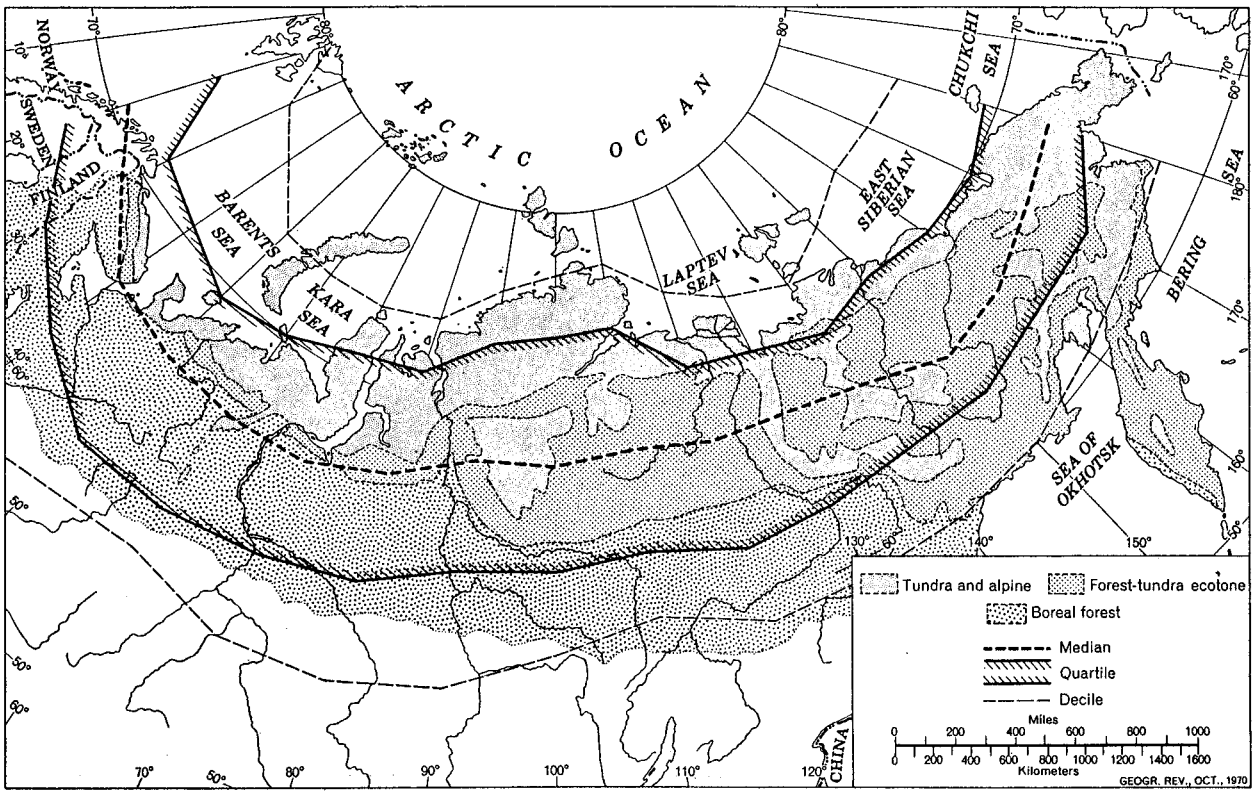

FIG. 2. The Arctic frontal zone over Eurasia during Jul as depicted by Krebs and Barry (1970), based on SLP analyses from 1952 through 1956.

they considered to represent the Eurasian Arctic frontal zone using daily SLP analyses for July of 1952–56. Lending credence to Bryson's (1966) work, an association was noted between the median frontal position and the tree line. However, in contrast to Reed and Kunkel (1960), they showed the frontal zone extending as an unbroken feature across the northern part of the Eurasian continent (Fig. 2). Their analysis technique was quite different, however. Instead of assessing frontal frequencies based on all observed fronts, they plotted the median, quartile, and decile ranges of only the northernmost fronts observed. Other studies include those of Yoshimura (1967), who presented findings similar to those of Reed and Kunkel (1960) based on July data, and Kurashima (1968), who noted a baroclinic zone in the vicinity of the Arctic coastline based on 1000–500-hPa thickness charts for June and August 1946–53 and 1955–56. Willis and Grice (1977) examined the wintertime Arctic front over Alaska and its effects on weather in Fairbanks, Alaska.

More recent studies using aircraft data collected during the winter season under the Arctic Gas and Aerosol Program (AGASP) (Shapiro et al. 1984, 1987; Shapiro 1985) presented clear evidence of Arctic jet streams with well-defined tropopause folds (as diagnosed from potential vorticity) between the lower (approximately 5 km) Arctic tropopause to the north and the higher (7 km) polar tropopause to the south. This led Shapiro et al. (1987) to propose a conceptual model of the meridional structure of the tropopause and principal jet streams that includes an Arctic front, hence harking back to the three-front Canadian analysis scheme.

It nevertheless seems that despite a fairly ample literature, there is as yet no universally accepted view as to what truly distinguishes ''Arctic'' from ''Polar'' fronts. When combined with the variety of terminology and study approaches employed, it becomes difficult to compare results from previous work. The existence of high-latitude fronts as separate from midlatitude fronts on a day-to-day basis is well established from aircraft studies (e.g., Shapiro 1985) and from vertical cross sections presented even in early synoptic atlases (Bolville et al. 1959). Krebs and Barry (1970) considered Arctic fronts to represent the northernmost frontal boundaries. This simple definition allows for fairly direct comparisons with the study of Barry (1967), who relied on Canadian analyses in which Arctic fronts also appear as the northernmost frontal features. However, the term Arctic frontal zone as used by Reed and Kunkel (1960) to describe a preferred region of frontal activity (implying the existence of an associated mean baroclinic zone) separate from frontal activity in midlatitudes was based on plotting any frontal surface observed. From

this analysis, Reed and Kunkel (1960) conclude that a separate Arctic frontal zone emerges in summer only. While seemingly at odds with Barry's (1967) view that the Arctic frontal zone can be defined in all seasons, the study approaches were fundamentally different.

The purpose of the present paper is to reexamine the concept put forth by Dzerdzeevskii (1945) and Reed and Kunkel (1960) of an Arctic frontal zone as a separate geographic region where frontal activity is preferred that can be identified from an analysis of monthly or seasonal frontal frequencies. We rely on fields from the National Centers for Environmental Prediction–National Center for Atmospheric Research (NCEP–NCAR) reanalysis (Kalnay et al. 1996). These data are used in an objective scheme to assess frontal frequencies. Results are compared with fields of the mean temperature gradient and vertical cross sections of the temperature gradient and zonal wind. Relationships between frontal frequencies and patterns of cyclogenesis, storm tracks and precipitation are addressed using improved datasets developed as part of previous efforts (Serreze et al. 1997; Serreze and Hurst 2000). Our study is restricted to the 20-yr period 1979–98, for which the reanalysis fields in northern high latitudes should be of higher quality than for earlier years due to the availability of a robust terrestrial rawinsonde network (Serreze et al. 1995) and sea level pressure data over the Arctic Ocean provided by networks of drifting buoys (Colony and Rigor 1993). We recognize, however, that errors may be present in the reanalysis fields even in areas with a high density of observations.

2. Frontal analysis

Compiling a 20-yr dataset of frontal activity clearly requires the application of automated methods. Hewson (1998) provides a review of objective frontal analysis schemes. Successful past efforts have employed a measure of frontal intensity termed the thermal front parameter (TFP) (e.g., Clarke and Renard 1966; Zwatz-Meise and Mahringer 1988; Japan Meteorological Agency 1988; Huber-Pock and Kress 1989, Blender and Schubert 2000). The TFP is defined as

$$-\nabla|\nabla\tau|(\nabla\tau/|\nabla\tau|),$$

where τ is a thermodynamic variable. It is evident that the TFP magnitude will be largest where there is a rapid change in the thermal gradient (the term on the left) with a large component parallel to the direction of the (unitized) thermal gradient.

For example, consider a temperature field in which the isotherms are oriented zonally, with the cold air to the north. Assume that the baroclinicity is concentrated in the middle of the field. For all locations, vectors of the unitized temperature gradient point south, toward higher temperatures. However, this is not true of vectors describing the change in the temperature gradient. North of the region of concentrated baroclinicity, these vectors point south, hence in the same direction as the unitized temperature gradient. Conversely, south of the region of concentrated baroclinicity, these vectors point to the north, hence parallel to, but in the opposite sense of the temperature gradient. In accord with normal convention, the minus sign of the left-hand term of the TFP equation acts to place the frontal boundary on the warm-air side of the concentrated baroclinic zone (corresponding to a ridge line in the field of TFP). More general cases are described by Hewson (1998).

Past studies have employed a variety of thermodynamic variables in the TFP calculation including thickness, equivalent thickness, potential temperature, equivalent potential temperature, and wet-bulb potential temperature at grid spacings on the order of 350 km. Generally, thresholds based on the magnitude of the TFP are applied to obtain the best agreement with fronts based on manual interpretation.

Given its successful use in past studies, its computational simplicity, and the rather coarse resolution of the NCEP–NCAR data (a 2.5° lat $\times$ 2.5° long grid), we use the TFP with a simple mask based on intensity. The TFP was computed at each grid point on a 6-hourly basis over the 20-yr period using 850-hPa temperatures for the region north of 30°N. The TFP was inspected at each grid point. If the value exceeded 1.0×10^3 K km^{-2}, then the values at the next higher and next lower latitudes along the same longitude were inspected to determine whether the value was a local maximum. If so, then the point was considered to be part of a front. The frequency of TFP values at each grid point passing this test was then determined on a monthly and seasonal basis over the entire 20-yr record and for individual years. To assist in plotting, the latitude–longitude grid of frontal frequencies was then transformed to a 250-km version of the National Snow and Ice Data Center (NSIDC) north polar equal-area scalable earth grid (Armstrong and Brodzik 1995) using a Cressman interpolation with a 500-km sphere of influence.

Our simple technique of locating TFP maxima (i.e., ridge lines) could fail if a front was oriented exactly along the same line of longitude for 5°, but this problem was rarely encountered. Given known problems of spectral distortion at high latitudes in the NCEP–NCAR moisture fields, we chose not to include moisture information (e.g., equivalent potential temperature) in the TFP calculations. The gradient fields needed to compute the TFP were calculated in spectral coordinates. The 850-hPa level was chosen as a compromise between the desire to examine low-level fronts while wanting to stay above the immediate boundary layer where the temperature field is strongly influenced by the model parameterizations.

Figure 3 provides examples of TFP fields for a winter and summer case (23 January 1988 and 6 July 1981, both at 1200 UTC). Here, we plot features for which the TFP exceeds 1.0×10^3 K km^{-2} The features are clearly rather broad (often more than 5° lat). As dis-

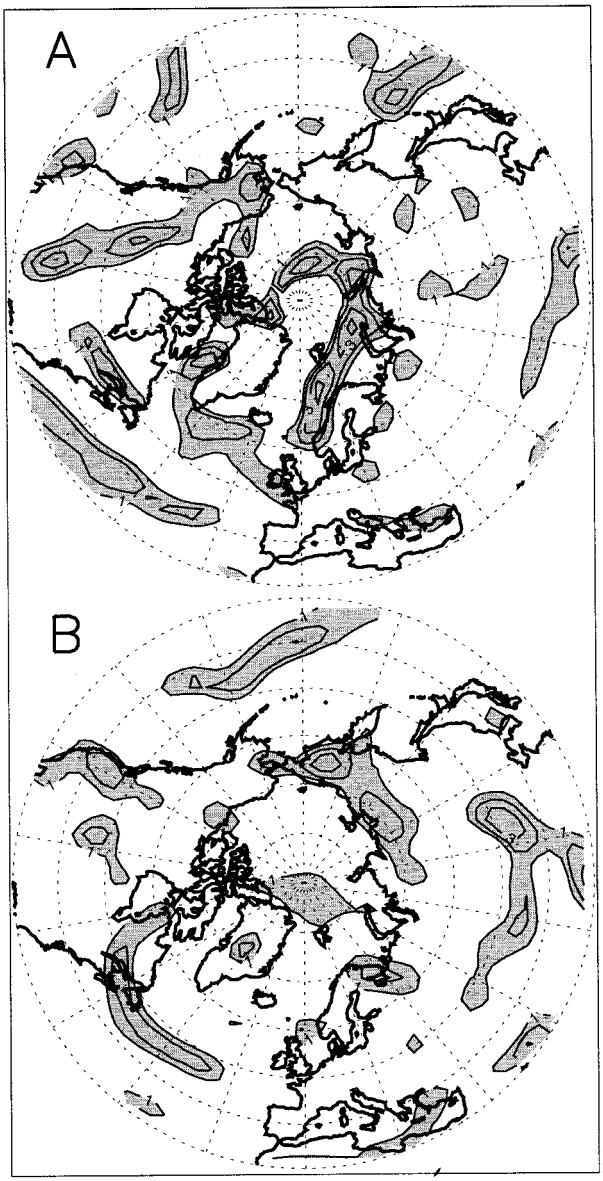

FIG. 3. Fields of the thermal front parameter at 1200 UTC for (a) 23 Jan 1988 and (b) 6 Jul 1981. Values above 1.0×10^3 K km^{-2} are shaded, with isolines plotted at the same intervals.

cussed, our assessments of frontal frequency are based on further processing of individual fields such as those in Fig. 3 to isolate the TFP maxima within these broad regions, which in most cases exceed 1.5×10^3 K km^{-2}. The most notable frontal feature in the January case is along the coast of Scandinavia and northern Eurasia and extending into the central Arctic Ocean, associated with a deep low pressure trough extending to the pole. Note the quasi-linear features over central and northeast North America as well as off the North American coast. Of note in the July case is the front along the northern shore of eastern Siberia, associated with the southern boundary of a cold anticyclone centered over the Eurasian side of the Arctic Ocean. Other well-defined fronts are found over the Pacific basin and off the east coast of North America, associated with the dominant storm tracks.

A number of comparisons were made with fronts depicted on NCEP surface analyses for the United States. With regard to major frontal features shown in these analyses, our threshold is a conservative one—continuous fronts on the NCEP analyses are typically depicted in the TFP field as discontinuous and frontal length is underrepresented. On the other hand, the TFP fields include features not seen in the operational analyses. These range from small ''bullseyes'' to linear features. While many of the smaller ones are transient, others persist from day to day and are associated with topography and established land–ocean temperature contrasts. The front along the west coast of North America in the July case, for example, is associated with the thermal contrast between the warm, elevated land surface and the colder ocean.

To obtain temperatures at pressure surfaces that lie below the earth's surface, the NCEP–NCAR reanalysis utilizes a downward extrapolation of temperature from the lowest model level, using a standard atmospheric lapse rate (6.5 K km^{-1}). This requires specification of the below-ground pressure heights, which also relies on temperature extrapolation (R. Kistler 2000, personal communication). Resulting errors in temperature fields can appear as spurious frontal features. The bullseye over central Greenland seen in the July case (common in summer charts) provides an example. Central Greenland lies at approximately 700 hPa, well above the 850-hPa level used in the frontal analysis, hence requiring considerable extrapolation.

A number of methods were explored to eliminate questionable features such as seen in Fig. 3 using different thermal variables in the TFP calculations, but these were not adopted. This decision stems from both the lack of a satisfactory way to deal with topography and land–ocean temperature contrasts as well as recognition as our study progressed that such effects are in fact important in understanding the development of the Arctic frontal zone. In the end, for the seasonal maps that follow shortly, we decided to simply mask out the obvious problem areas. These correspond to central Greenland (an elevated cold plateau), Northern Africa (related to strong surface heating), lower latitudes of the Eurasian landmass and up to 50°N along the longitudes of the Himalayas and the Tibetan Plateau, as well as the southwestern United States (regions with extreme topography and/or strong surface heating).

Experiments were also performed with a more robust technique described by Hewson (1998). In this approach, ''potential fronts'' are first located by finding where the Laplacian (i.e., the 2D curvature) of the magnitude of the thermal gradient is zero. Locations with zero divergence are then compared to limiting values of two masking functions, the first being the TFP and

the second a measure of the strength of the baroclinic zone adjacent to the front. While much more computationally intensive, results were found to be sensitive to the same problems encountered using the simpler TFP approach. It is worth noting that the examples shown by Hewson (1998) were restricted to open-ocean regions where frontal analysis is greatly simplified. McInnes et al. (1994) find that with high-resolution (50 km) data, problems of topography and land–ocean contrasts can be in part circumvented through identification of vorticity maxima to locate the wind shift line. Planned studies using output from the ARCSyM regional model (Lynch et al. 1995) will make use of this quantity. As suggested by Hewson (1998), we may also explore the use of a terrain-following vertical coordinate system (sigma levels).

3. Seasonal aspects of frontal activity

Figure 4 shows frontal frequencies for the four calendar seasons. Frequency is expressed as the mean number of fronts day^{-1}. For example, a frequency of 0.10 means a front was present on 10% of days. To aid in interpretation, we display in the same figure fields of the mean 850-hPa temperature and the magnitude of the temperature gradient in K (100 km)$^{-1}$ based on the 20-yr mean temperature field.

Although the winter frontal frequency field is rather noisy, frontal frequencies exceeding 0.10 and locally higher are found over most of North America except northeastern Canada, where the mean temperature gradient is weak and temperatures are lowest. A distinct band with frequencies of 0.10–0.20 is found extending northeast over the Atlantic basin, associated with the eastern North American jet and its attendant storm track, and then continuing northeast over northern Europe. A similar oceanic feature, extending beyond the latitude bounds in Fig. 4, is found over the Pacific Basin in association with the East Asian jet and the Pacific storm track. Note the fairly high frequencies over extreme northeastern Eurasia and the northern Pacific Ocean, largely contiguous with the zone of high frequencies over Alaska and extending south. Frontal activity over these regions appears to some extent as ''separate'' from the frontal activity further south in the Pacific basin.

As expected, there is considerable similarity between the patterns of frontal frequency and of the magnitude of the gradient of the mean temperature field. One can see how the maxima in frontal frequency are placed on the warm side of mean baroclinic zones. For example, the frontal zone over the Atlantic basin lies south of the maximum temperature gradient this area. A pattern similar to that calculated from the 6-h TFP maxima can be obtained by computing a single TFP field from the mean temperature field. The winter gradient fields also exhibit features associated with topography and land–ocean contrasts. For example, the area of high frontal frequencies extending west of the Pacific coast of North America is associated with the contrast between the cold interior and warm ocean, seen by the ''kink'' in the winter 850-hPa temperature field along the coast. Very strong temperature gradients are found in association with the Himalayas and the Tibetan Plateau, and in turn associated with a high frequency of fronts in the region masked in Fig. 4.

The high frequency of fronts east and northeast of Greenland is not surprising. The baroclinicity in this region (corresponding to the Icelandic low) is made strong by numerous factors, including the contrast between the warm northward-flowing North Atlantic Drift current, the cold southward flowing East Greenland current, proximity to the sea ice margin and the reservoir of cold Arctic air to the north. Note the distinct separation between this area of frequent frontal activity and the relative maximum in fronts farther south associated with the eastern North America jet. In this respect, we could consider the area east and northeast of Greenland in the context of a separate wintertime Arctic frontal zone.

As compared with winter, spring shows a decline in activity over the Atlantic basin, with a northward migration of activity over the Pacific basin. Frequencies are high over Northwestern North America, but with a general shift in activity toward the interior, resulting in a well-defined band of high frequencies extending along the eastern flank of the Rocky Mountains and into Alaska. A local maximum is found centered at about 65°N, which considering the resolution of the NCEP–NCAR data appears as collocated with the Brooks and Mackenzie ranges. As for winter, the pattern over Eurasia is rather noisy. The region of high frontal frequencies over the extreme northeastern part of the continent is less pronounced (note the weaker baroclinicity in this area as compared with winter). Some separation is evident between the frontal activity over Alaska and that to the south in the Pacific Basin.

During the summer, surface heating and elevated topography give rise to very high frontal frequencies over northern Africa, the highlands of Iran, Afghanistan, and the Tibetan Plateau, which have been masked in Fig. 4. These problems are evident in the temperature gradient fields. Spuriously high frontal frequencies are also found

→

FIG. 4. (a) and (b) (top) Frontal frequencies (fronts day^{-1}), (middle) mean 850-hPa temperatures (K), and (bottom) gradients of the mean 850-hPa temperature field [K (100 km)$^{-1}$] for the four calendar seasons. Areas masked in the frontal frequency maps represent regions with known problems related to extreme topography and surface heating. Areas where the mean temperature gradient exceeds 0.5 K 100 km^{-1} are shaded in yellow.

(a)

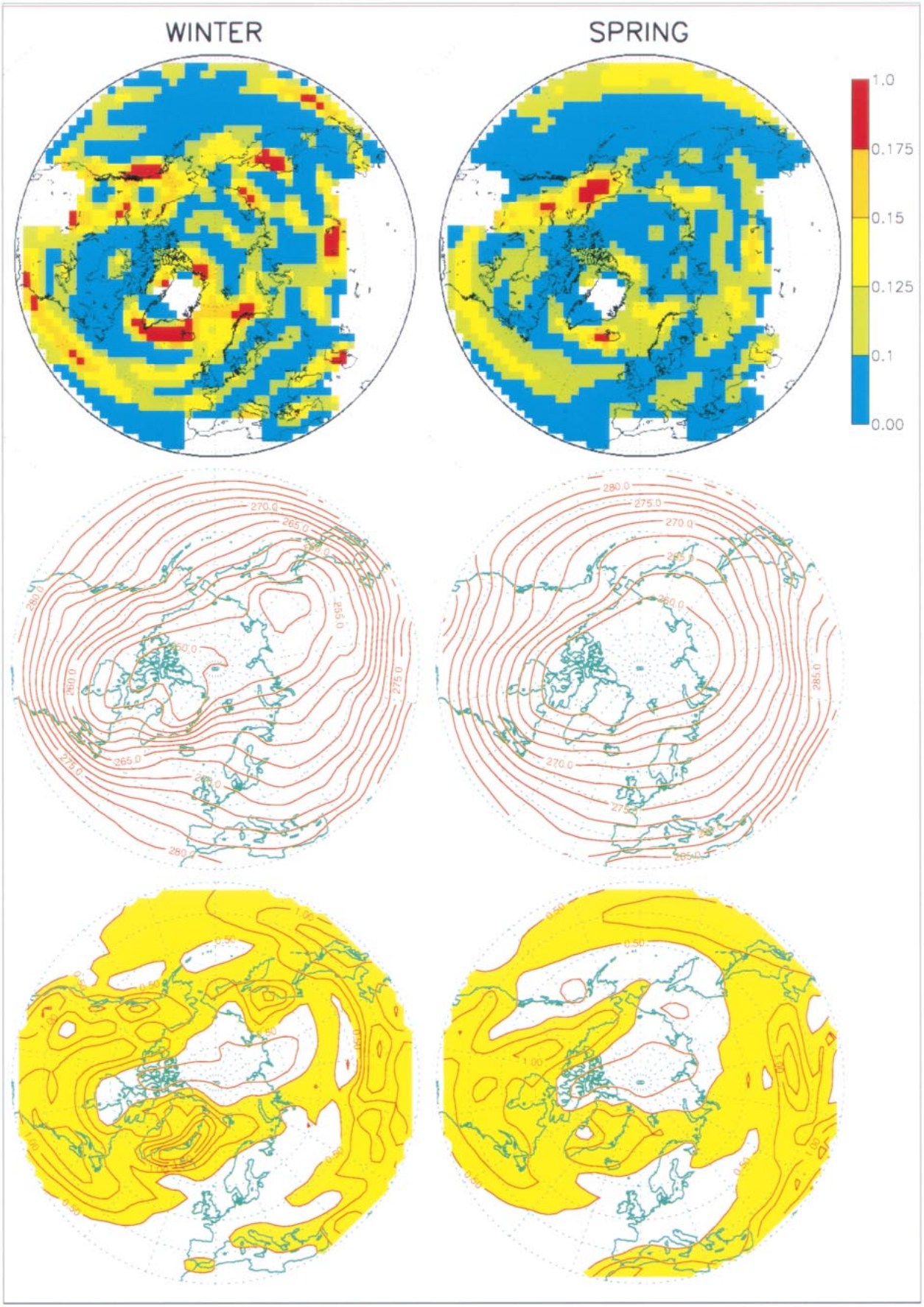

(b)

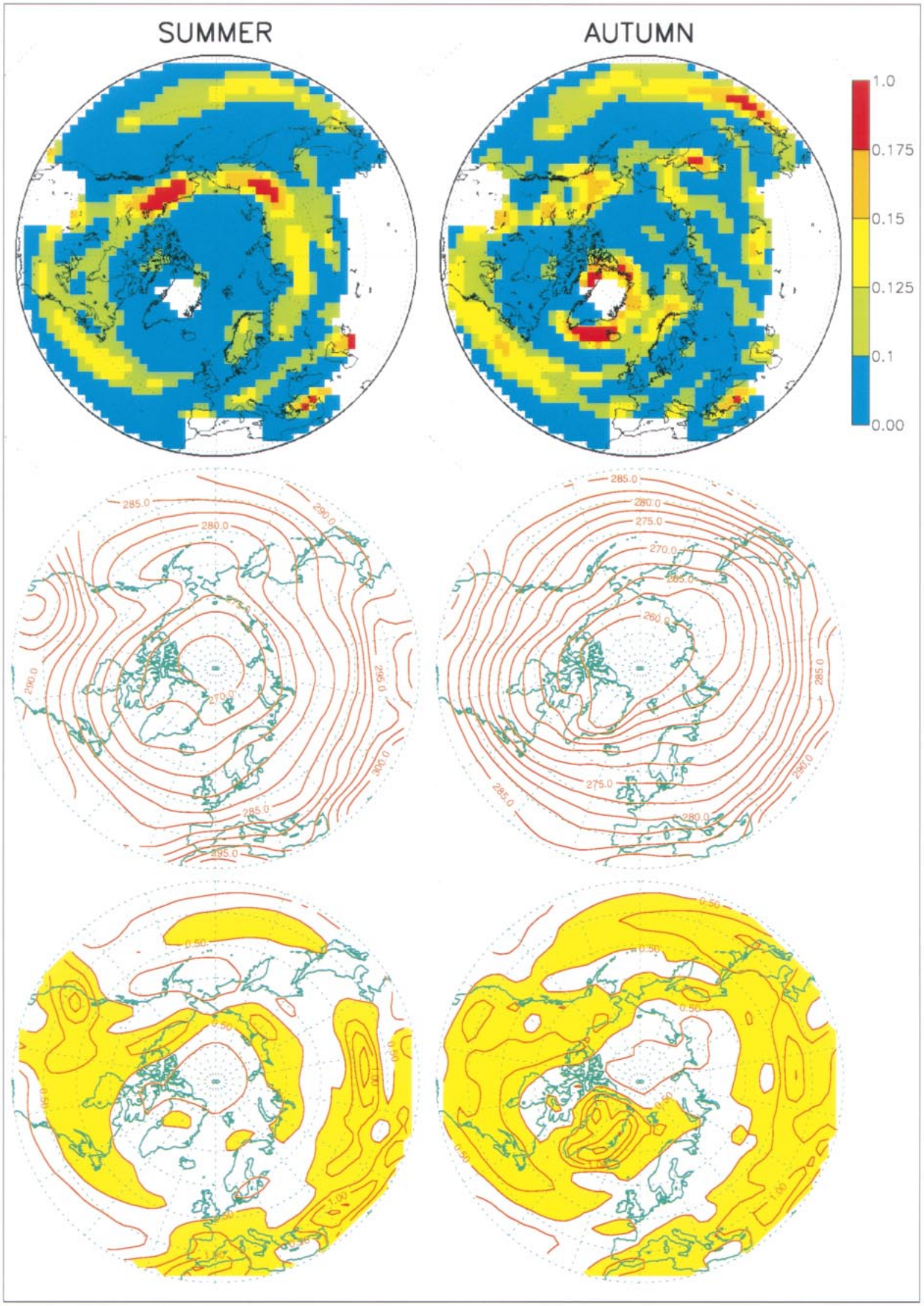

over the southwestern United States. One can see clearly from the mean temperature and gradient fields how this relates to the strong heating of the elevated plateau, giving rise to a baroclinic zone to the north.

With respect to the present study, the most interesting feature of summer is the development of a well-defined, zonally oriented band of high frontal frequencies over northern Eurasia. In essentially extending across the continent, this feature appears very similar to the summertime Arctic frontal zone depicted by Krebs and Barry (1970) (Fig. 2). The highest frontal frequencies (locally exceeding 0.175) are located over central and eastern Eurasia, a feature not shown in Reed and Kunkel's (1960) analysis. Reed and Kunkel (1960) also depict a separate frequency maximum at lower latitudes extending from Italy eastward to about 130°E representing the polar frontal zone (Fig. 1). We see an analogous feature (similar to that shown for winter), but problems with topography make it difficult to assess its eastward extension. The high-latitude Eurasian frontal zone is associated with a mean baroclinic zone aligned roughly along and extending inland from the Arctic Ocean coastline. Not surprisingly, a single TFP field calculated from long-term mean fields results in a similar pattern. Reed and Kunkel (1960) view the summer Arctic frontal zone in Eurasia as distinct from the region of high frontal frequencies in midlatitudes of the Pacific Basin. While such separation is clearly borne out in our results, we stress from previous discussion that separation is also evident to some extent in winter.

The relative maximum in frontal frequencies over Alaska seen in winter and spring has strengthened in summer, and appears as contiguous with the Eurasian frontal zone. Again considering the resolution of the NCEP–NCAR data, the location of the frequency maximum over Alaska corresponds to that shown by Reed and Kunkel (1960). There is some evidence of an extension of relatively high frontal frequencies from Alaska and eastward across Hudson Bay as shown by both Reed and Kunkel (1960) and Barry (1967).

The well-defined Eurasian frontal zone seen in summer breaks down in autumn while the high-latitude feature over Alaska is still present in a weakened form. The Alaskan feature, while best expressed in summer, hence persists throughout the year. Frontal frequencies increase in the Pacific and Atlantic basins, with the redevelopment of a separate region of frontal activity in the vicinity of Greenland. Overall, the patterns of autumn frontal frequency most closely resemble those for winter.

To focus further on the summer pattern, Fig. 5 plots frontal frequencies by longitude for June, July, and August averaged from 62.5° to 67.5°N along with the corresponding coefficient of deviation based on monthly frequencies over the individual years of the 1978–98 record. Frontal frequencies over the Eurasian sector are highest at about 140°E and maximized during June (>0.20). For the Alaskan sector, frequencies exceed 0.15 for all three summer months, and exceed 0.20 for both June and July. Note also the low (locally <20%) coefficient of deviation associated with the frequency maxima (i.e., the standard deviation is only about 20% of the mean), pointing to the persistence of these frontal zones from year to year. Further investigation reveals no obvious temporal trends in summer frontal frequency over either the Eurasian or Alaskan sectors.

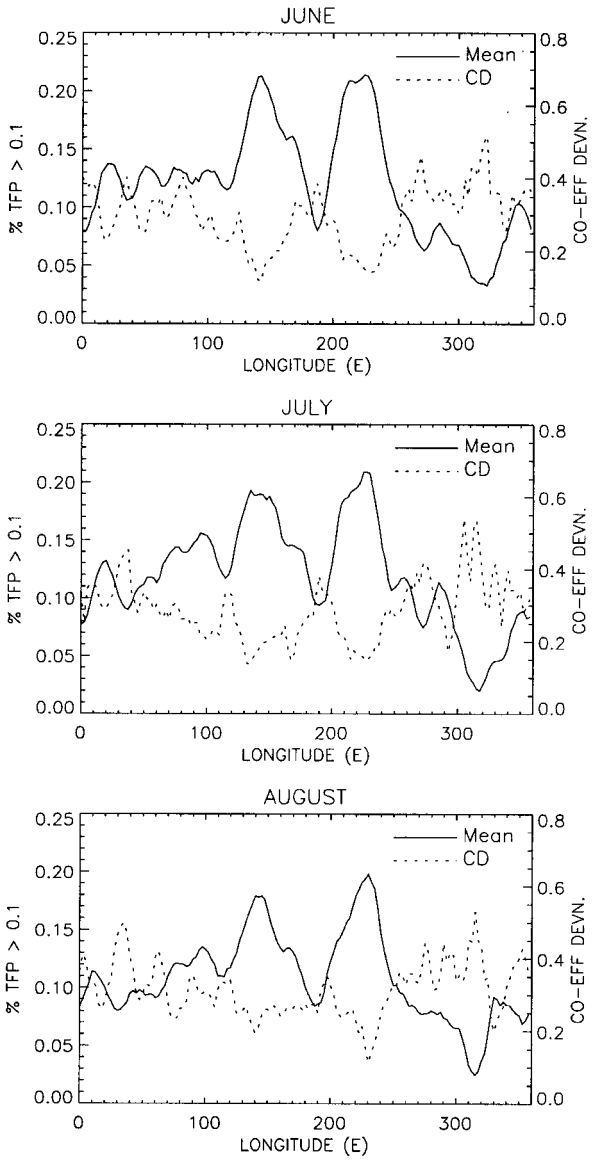

FIG. 5. Frontal frequency (fronts day^{-1}) averaged from 62.5° to 67.5°N and coefficient of deviation (dimensionless) for Jun, Jul, and Aug.

4. Diagnosis

If we consider the Arctic frontal zone(s) from a geographical definition as area(s) of preferred frontal activity emerging as separate from the polar frontal zone in midlatitudes, it is evident from Fig. 4 that such a distinction can be made for Alaska in all seasons and

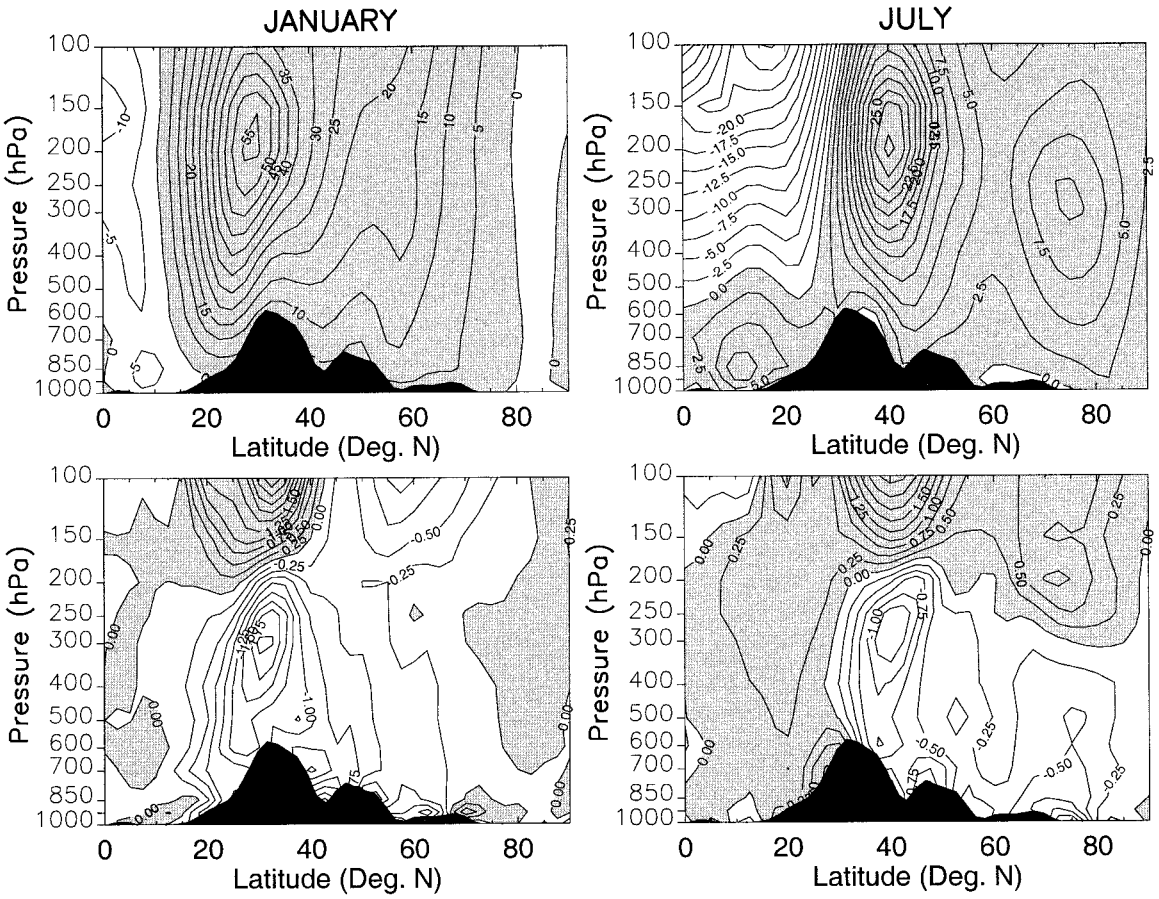

FIG. 6. (top) Mean zonal winds (m s^{-1}) and (bottom) meridional temperature gradient [K (100 km)$^{-1}$] from the equator to the pole at 100°E for Jan and Jul. Positive values are shaded. Data below the local surface (based on the NCEP–NCAR topography) are masked.

for northeastern Eurasia in every season except spring. For winter, a distinct separation is also found between frontal activity east and northeast of Greenland and that farther south in the Atlantic basin. Taken in this context, the Arctic frontal zone is not simply a summer feature. Summer does, however, contrast sharply with other seasons in terms of the existence of a well-defined frontal zone extending across the Eurasian continent.

From Fig. 4 and inspection of 850-hPa height fields (not shown), it is evident that development of the summer Eurasian Arctic frontal zone is associated with a pronounced seasonal change in the regional circulation. During winter, the Eurasian sector north of about 60.0°N and from 80° to 150°E lies well north of the baroclinicity associated with the East Asian trough. To the west and east, the circulation has a strong meridional component. The circulation over most of Eurasia becomes distinctly zonal in summer. At longitudes 80°–150°E this is accompanied by a general northward shift of baroclinicity. The transition between the winter and summer circulation is evident in the fields for spring. This seasonal change is seen in the development of a zonal band of high frontal frequencies. As seasonal changes in the temperature structure are less pronounced over the Alaskan sector, it follows that seasonal changes in frontal frequency are less well expressed.

It is interesting from Fig. 4 that the mean baroclinicity over northern Eurasia and Alaska during summer is strongest along and just south of the Arctic Ocean coastline. We further note that near the surface, temperatures over the cold Arctic Ocean are within several degrees of the freezing point, while those over the adjacent snow-free land are on the order of 10°–20°C, likely associated with considerable vertical mixing. A reasonable explanation is that the coastal baroclinic zones and associated frontal maxima manifest this differential heating. Recall that a role of differential heating was suggested in the early studies of Dzerdzeevskii (1945) and Kurashima (1968). Taken in this context, the summer frontal zones could be considered analogous to the prominent frontal zone near Greenland seen in winter, spring, and autumn (Fig. 4). As discussed, this feature is consistent with strong differential heating across large gradients in sea surface temperature. In reflecting forcing by the surface on the regional circulation, this feature, like the Arctic frontal zone, can be distinguished from the areas of pronounced

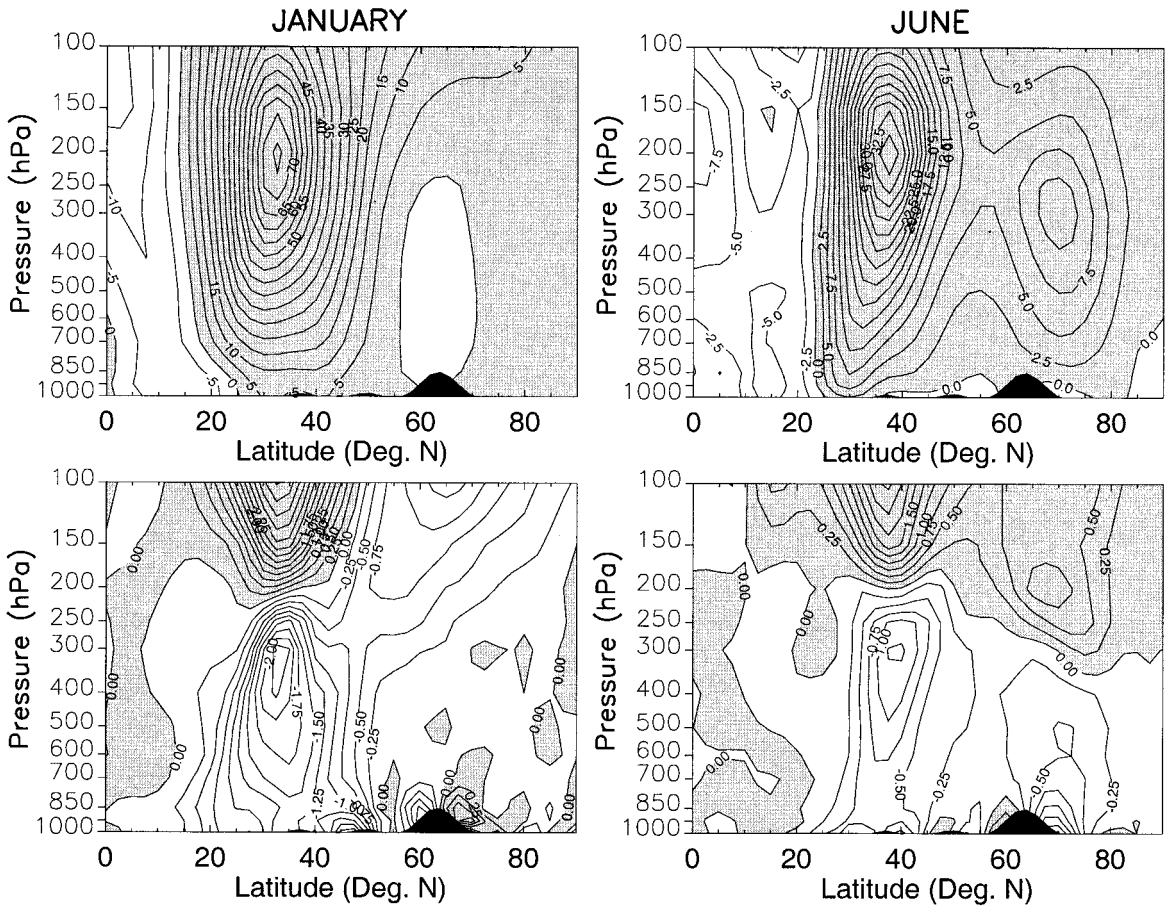

FIG. 7. (top) Mean zonal winds (m s^{-1}) and (bottom) meridional temperature gradient [K (100 km)$^{-1}$] from the equator to the pole at 140°E for Jan and Jun. Positive values are shaded. Data below the local surface (based on the NCEP–NCAR topography) are masked.

frontal activity in the midlatitudes of the Atlantic and Pacific basins, which are more clearly a function of the large-scale circulation (i.e., the eastern North American and East Asian jet systems).

To test the idea of differential heating and to help further determine the extent to which the summertime Arctic frontal zone can be considered distinct from frontal activity in midlatitudes, it is useful to examine vertical cross sections of the mean temperature gradient and winds throughout the troposphere. To this end, vertical cross sections (using 12 levels from 1000 to 100 hPa) of the mean zonal wind and the meridional temperature gradient from the equator to the pole based on 20-yr means (1979–98) were compiled at every 20° of longitude for each month. For each longitude, plots for January were compared to the summer month (variously June–August, depending on longitude) with the highest frontal frequency averaged over latitudes 62.5°–67.5°N (based on the same data used to construct Fig. 5). Here, we show selected contrasting cross sections for 100° and 140°E (Eurasia) and for 140° and 80°W (North America). Data below the local surface (based on the NCEP–NCAR topography) are masked out.

Longitude 100°E (Fig. 6) cuts through a part of the summer Eurasian frontal zone with frontal frequencies between 0.125 and 0.150. The mean zonal wind section for January is characterized by a single jet at about 30°N (55 m s^{-1}). The temperature gradient is maximized at about 300 hPa, and while bearing characteristics of the subtropical jet, statistical averaging with polar front jets is evident in the baroclinicity at lower levels and its extension to the north. High-latitude frontal activity along this longitude is strongest in July. As compared to January, the midlatitude jet feature has migrated poleward in July and weakened to about 30 m s^{-1}. The low-level westerly jet at about 15°N and the easterlies aloft are associated with the east Asian summer monsoon. Of interest to the present work, however, is the development of a distinct wind maximum at about 75°N (10 m s^{-1}) centered at the 300-hPa level. The baroclinicity associated with this wind maximum extends from 60° to 80°N up to 400 hPa, sharpest at low levels very close to the Arctic Ocean coast (77°N at this longitude). The corresponding zone of high frontal frequencies is found from about 60° to 70°N, on the warm side of the baroclinic region.

Longitude 140°E (Fig. 7) cuts through the region

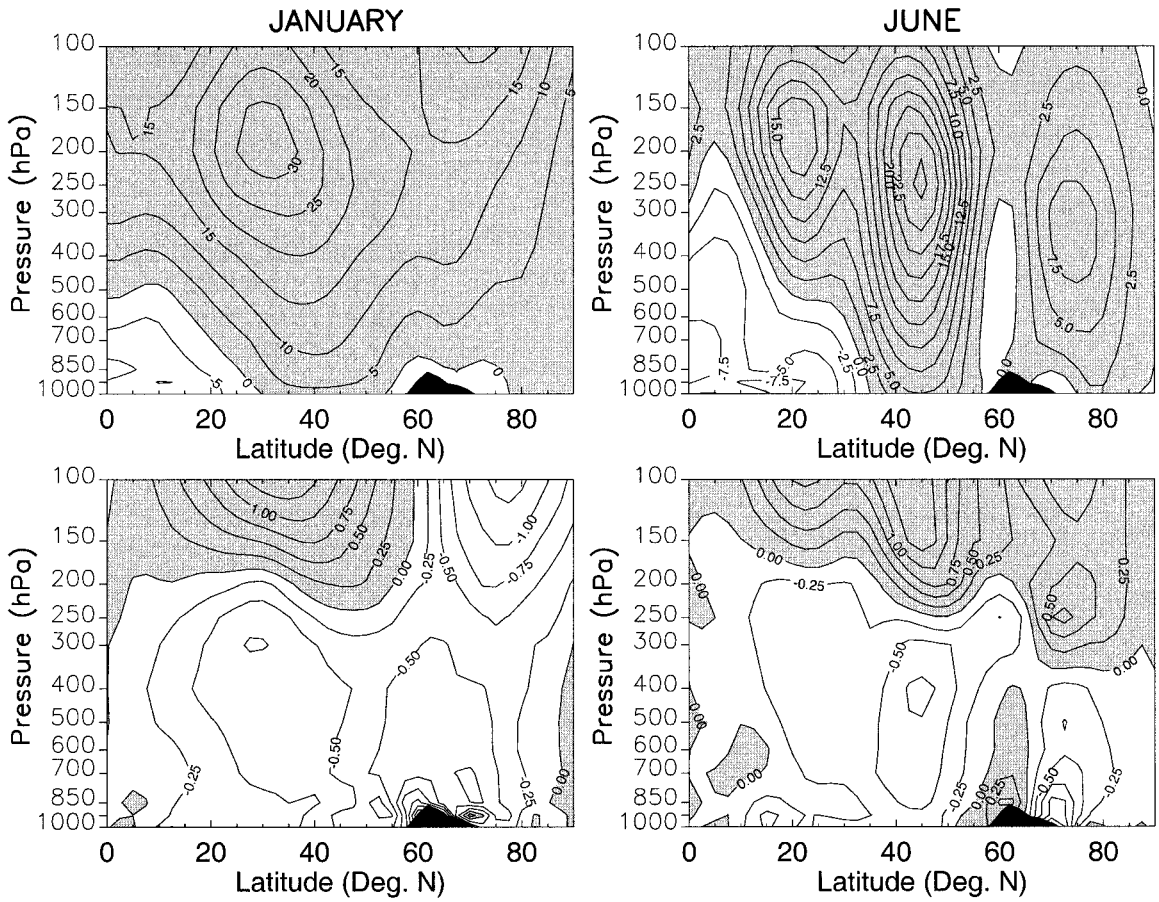

FIG. 8. (top) Mean zonal winds (m s^{-1}) and (bottom) meridional temperature gradient [K (100 km)$^{-1}$] from the equator to the pole at 140°W for Jan and Jun. Positive values are shaded. Data below the local surface (based on the NCEP–NCAR topography) are masked.

where the summer Eurasian frontal zone is best expressed. The zonal wind cross section for January again shows a single jet with a core velocity of about 75 m s^{-1}. Note the high-latitude baroclinicity at lower stratospheric levels, capturing the lower end of the polar night jet. Within the middle to lower troposphere, the temperature gradient north of 50°N is weak, but with a small, sharp feature at 60°N corresponding to the coast of the Sea of Okhotsk and another of opposing sign at about 70°N near the Arctic Ocean coastline. This latter feature may reflect heat fluxes through coastal leads and polynyas increasing temperatures relative to the nearby landmass (a similar coastal feature is seen in the January plot in Fig. 6). At 140°E, the Arctic frontal zone is best expressed during June. The June zonal wind cross section is dominated by a jet at about 35°N, about half as strong as that for winter, but with a weaker, separate 300 hPa wind maximum (10 m s^{-1}) at 70°N. Again, this can be associated with a distinct high-latitude baroclinic zone extending to 400 hPa, maximized at low levels at about 70°N and close to the latitude of the Arctic Ocean coast (72.5°N).

Longitude 140°W (Fig. 8) cuts through Alaska, where the high-latitude frontal zone is again well expressed. For January, a single jet (30 m s^{-1}) is found at about 30°N. The lower end of the polar night jet is seen at about 70°N, and is clearly evident in the temperature cross section. A somewhat separate region of baroclinicity is found from 55° to 75°N, particularly sharp at low levels at about 62.5°N, corresponding to the southern coast of Alaska and reflecting the land–ocean contrast in this region. This is seen in Fig. 4 as a high frequency of frontal activity but is not associated with a jet core aloft. Note also the small region along the northern coast where the gradient at lower levels is reversed, similar to that seen in the January cross sections for 100° and 140°E. By sharp contrast, June reveals a subtropical jet at about 25°N, a polar jet at about 45°N, and a third Arctic jet at about 70°N. There is a fairly sharp baroclinic zone at about 70°N, again close to the latitude of the Arctic Ocean coast. Along the southern coast of Alaska, the gradient is reversed, indicative of heating of the land surface. The three-jet structure revealed in Fig. 8 is also present in the July and August fields. The high-latitude jet core is actually strongest in August. Note the clear reduction in tropopause height to the north associated with each feature.

In eastern north America, the high-latitude summer

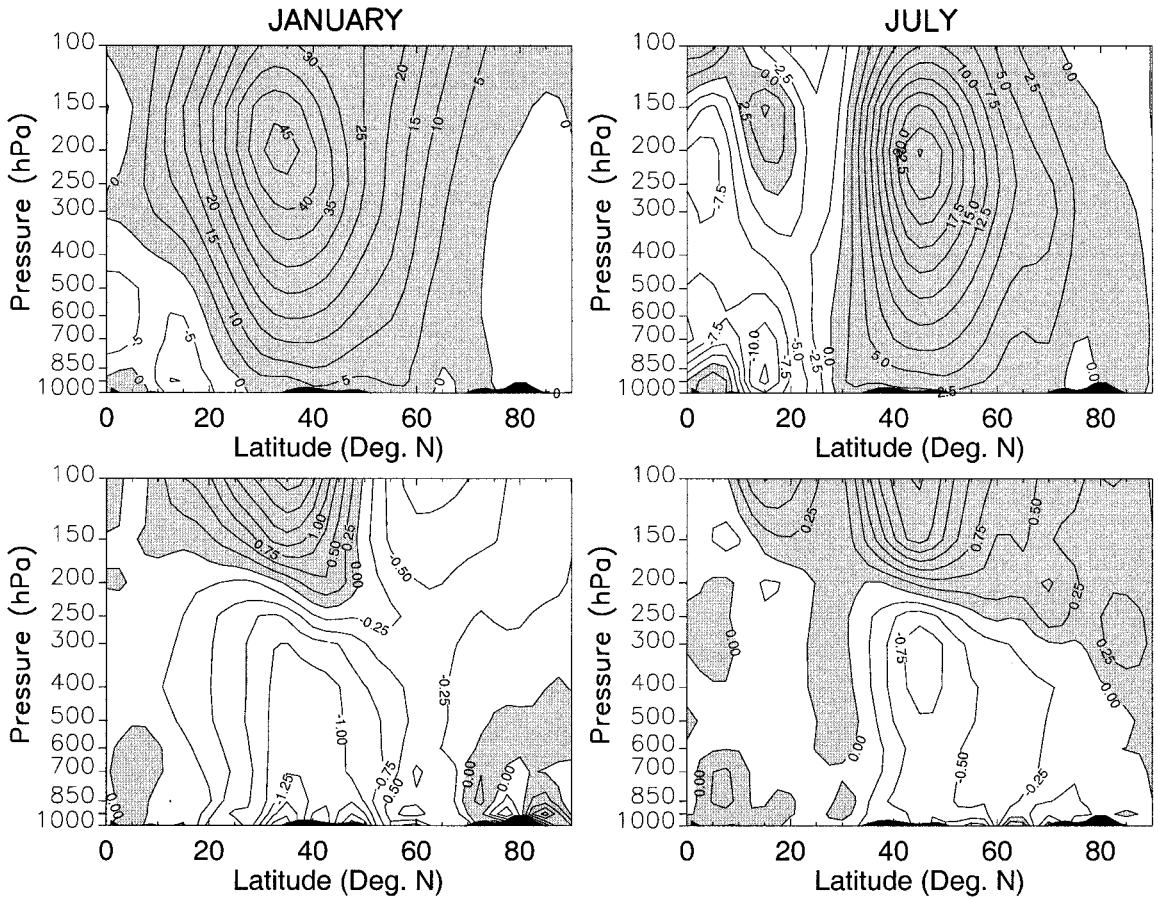

FIG. 9. (top) Mean zonal winds (m s^{-1}) and (bottom) meridional temperature gradient [K (100 km)$^{-1}$] from the equator to the pole at 80°W for Jan and Jul. Positive values are shaded. Data below the local surface (based on the NCEP–NCAR topography) are masked.

frontal zone is comparatively weak (Fig. 4). At 80°W (Fig. 9), the January cross section shows a single jet at about 35°N, with the associated baroclinicity increasing toward the surface. July also shows a single jet feature, but shifted north to about 50°N and about half as strong as its winter counterpart. There is no evidence in July of a pronounced baroclinic zone along the Arctic coast (about 83°N at this longitude).

These cross sections reveal that while in terms of the frequency of fronts, some separation between the Arctic frontal zone and the polar frontal zone to the south is seen in all seasons for those longitudes corresponding to the Pacific basin, it is only during summer that there exists a fairly deep baroclinic zone in high latitudes and associated wind maxima in the upper troposphere. The cross sections also lend credence to the idea that a key aspect of the development of the Eurasian summer frontal zone is the existence of north–south heating contrasts between the Arctic Ocean and snow-free land. This is evident in the close agreement between the region of maximum baroclinicity and the Arctic coastline and the associated upper-level wind maxima. The role of differential heating is further supported by the cross sections through Alaska (140°W). Along this longitude, the high-latitude frontal zone is basically a year-round feature, and in a mean sense, the isotherms are always parallel to the coast (Fig. 4). However, the coastal baroclinic zone strengthens during summer, consistent with heating of the snow-free land surface. One can also see how along this longitude the low-level baroclinicity in January is strong near the southern Alaskan coast, associated with the contrast between the snow-covered land and relatively ice-free ocean. By contrast, for July in the same area, the land is warmed relative to the ocean, and the temperature gradient is reversed.

Similar reasoning helps to explain the comparatively weak summer frontal zone over eastern Canada. The baroclinicity in Canada during summer is concentrated along the descending arm of the western North American ridge, roughly along the southern boundary of the Canadian Arctic Archipelago (Fig. 4). The Archipelago is a heterogeneous landscape with a combination of land, sea, and ice-covered channels, acting to inhibit differential heating such as seen along Eurasia where the land–ocean boundary is sharply defined.

To further examine the existence of thermal contrasts between the land and ocean, a simple algorithm was developed to find the location of the maximum tem-

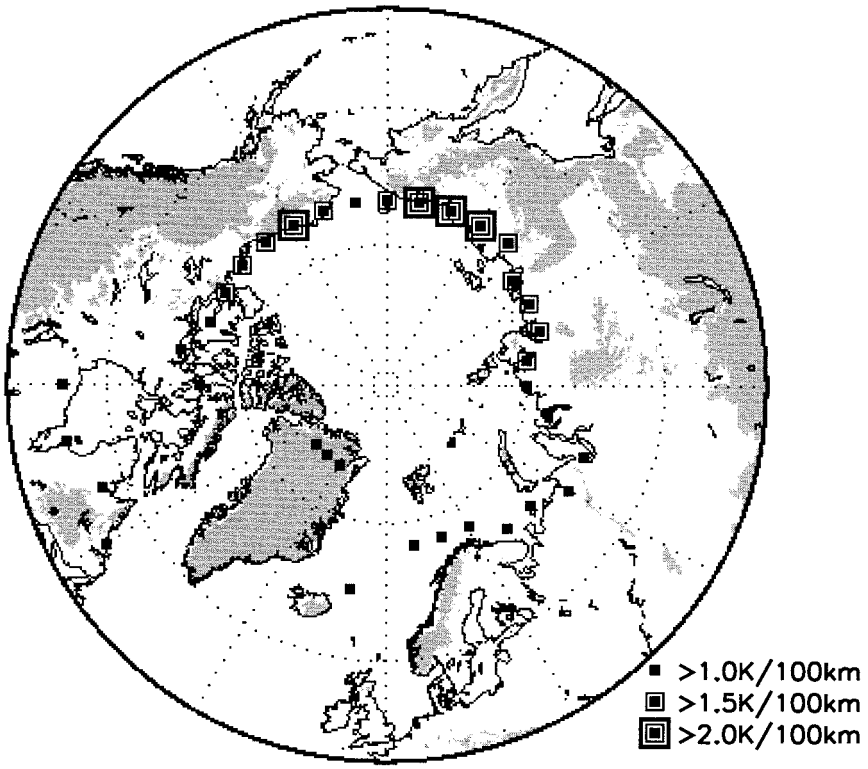

FIG. 10. Location of the maximum meridional temperature gradient north of 50°N for Jul. Points are only plotted at longitudes for which the gradient exceeds 1.0 K (100 km)$^{-1}$. For all plotted points the maximum temperature gradient is found at the 1000-hPa level. Also shown are areas with elevations above 500 m (shaded), based on ETOPO-5 data.

perature gradient (based on the 20-yr mean temperature fields) and its magnitude at every 10° long for the region north of 50°N. For June, July, and August, a location can always be found from 10°E eastward to from 110° to 80°W (depending on the month) where the poleward gradient exceeds 1.0 K (100 km)$^{-1}$. The gradient is always largest at the lowest analysis level (1000 hPa). At most longitudes, the maximum 1000-hPa temperature gradient is close to the coast and can be associated with wind maxima in the upper troposphere. As expected, the baroclinicity for all summer months is strongest at those longitudes where frontal frequencies are highest. Results for July are presented in Fig. 10. These Arctic Ocean coastal features are not observed in winter months. Not surprisingly, winter does show strong-low baroclinicity in the Greenland Sea along the sea ice boundary, consistent with the winter frontal activity in this region.

One other factor to consider is topography (cf. Reed and Kunkel 1960). Comparisons between the summer map of frontal frequencies in Fig. 4, and the simplified topography in Fig. 10 reveals the Eurasian summer frontal zone to be best expressed in the broad v-shaped lowland area bounded by the Verkhoyansk, Cherskogo, and Gydan ranges. As mentioned earlier, the frontal zone over Alaska corresponds to the Brooks and Mackenzie ranges. An apparent link between where the summer frontal zone is best expressed and significant topography is perhaps more evident in the cross sections shown in Figs. 7 and 8. Investigations of possible dynamic contributions of topography (e.g., cold air damming) are ongoing via model sensitivity studies.

5. Associations with cyclogenesis, cyclone tracks, and precipitation

An automated cyclone detection and tracking algorithm has recently been applied to the NCEP–NCAR reanalysis 6-h SLP fields. Cyclones are identified using a series of search patterns, testing whether a gridpoint sea level pressure value is surrounded by gridpoint values at least 1-hPa higher than the central point being tested. Cyclones are tracked by comparing system positions on subsequent 6-hourly charts using a nearest-neighbor algorithm. Cyclogenesis is taken at the first appearance of a closed (1 hPa) isobar. Earlier versions of the detection and tracking algorithm based on 12-h National Meteorological Center (NMC, now known as NCEP) pressure data are described by Serreze (1995) and Serreze et al. (1997).

Figure 11 shows cyclogenesis counts for winter (December–February) and summer (July–August) based on

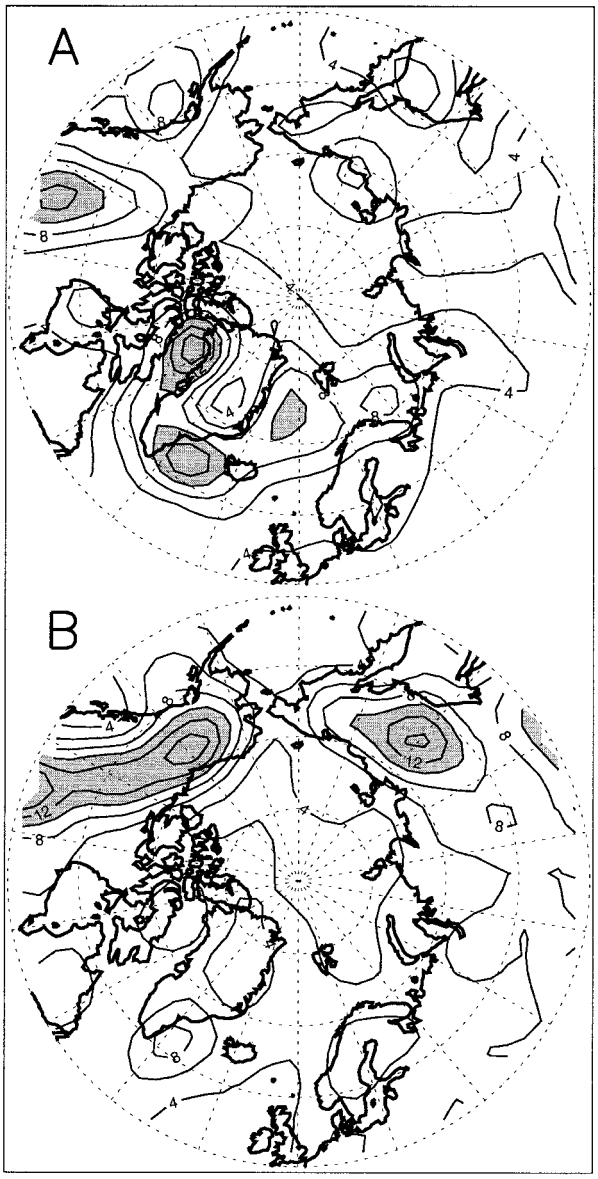

FIG. 11. Total counts of cyclogenesis for (a) winter and (b) summer over the period 1979–97 in grid cells of 62 500 km^2 (250 km $\times$ 250 km). Areas with more than 10 occurrences of cyclogenesis are shaded.

the NCEP–NCAR data over the period 1979–97. Only those systems lasting at least 12 h (two charts) are considered. A sharp seasonal contrast is evident in the distributions of cyclogenesis. During winter, cyclogenesis is most common east of Greenland, the Barents Sea, in Baffin Bay, and western Canada. By contrast, cyclogenesis during summer exhibits well pronounced maxima over east-central Eurasia as well as over Alaska and extending southeast. These features were remarked upon in several earlier studies (Whittaker and Horn 1984; Serreze 1995; Serreze et al. 1997). There is a close correspondence between the highest counts of summer cyclogenesis and the maxima in frontal frequencies (Fig. 4). Our interpretation is that the baroclinicity associated with the summer frontal zones enhances cyclogenesis. Closer inspection of the data also suggests a possible contribution by leeside cyclogenesis processes. Within the resolution of the reanalysis fields, the summer cyclogenesis maximum in Eurasia appears associated with the lee of the Verkhoyansk range, while the maximum over northern North America roughly corresponds to the lee of the Mackenzie Range and northern Rocky Mountains. Leeside effects could help explain why the North American cyclogenesis maximum exhibits a more pronounced southward extension than does the region of high frontal frequencies in this sector.

Previous studies (Reed and Kunkel 1960; Serreze and Barry 1988; Serreze et al. 1997) argued that cyclones generated along the Arctic frontal zone have a tendency to track into the Arctic Ocean where they occlude and fill. Serreze et al. (1989) argued that once in the Arctic Ocean, these systems have significant impacts on the circulation of the underlying sea ice cover, promoting periods of sea ice divergence that represent areas of new ice production in autumn. However, none of these studies attempted a systematic tracking of cyclones to assess source regions. To clarify this issue, tracks of the cyclones originating in the Eurasian and Alaskan summer frontal zones are displayed in Fig. 12 for June, July, and August. While systems generated along the Eurasian frontal zone tend to track eastward, many do in fact enter the Arctic Ocean. This does not appear to be true of systems generated along the Alaskan frontal zone, which primarily track southeastward into the Canadian Arctic Archipelago.

One expects that the summer frontal activity over Eurasia and Alaska and associated cyclogenesis will manifest itself in precipitation. This relationship is borne out in Fig. 13, which plots by longitude the fraction of mean annual precipitation falling in summer (June–August) along with the summer frontal frequency. Both variables are averaged over latitudes 62.5°–67.5°N. Precipitation is based on a gridded product that uses the Legates and Willmott (1990) climatology as a first guess, adjusted by gauge-corrected station data for Eurasia and Canada. An earlier version of this climatology is described by Serreze and Hurst (2000). At 140°E, where the Eurasian frontal zone is best expressed, nearly 60% of annual precipitation falls during summer. Where the Alaskan frontal zone is best expressed, over 50% of precipitation falls during summer.

6. Summary and conclusions

From a purely thermal argument based on calculations of a thermal front parameter (TFP) on a 6-hourly basis using 20 yr (1979–98) of 850-hPa data from the NCEP–NCAR reanalysis, we demonstrate the development during summer of a band of high frontal frequencies along Eurasia from about 60° to 70°N, best expressed over the eastern half of the continent. A sim-

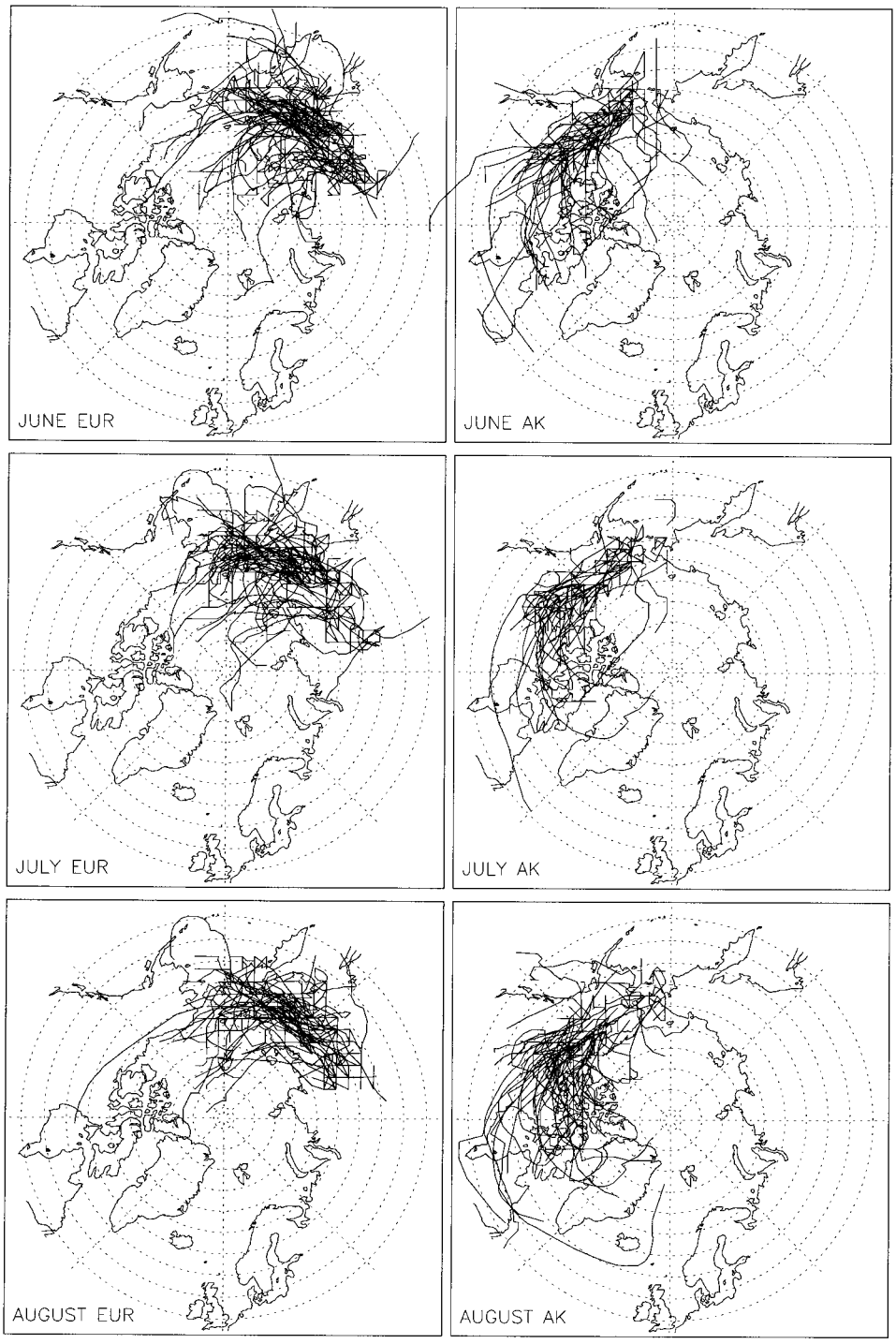

FIG. 12. Tracks of cyclones originating in the Eurasian and Alaskan frontal zones for Jun, Jul, and Aug over the period 1979–97.

ilar frontal zone is found over Alaska. Although best expressed in summer, the Alaskan feature is present year-round, representing the northern end of a belt of high frontal frequencies extending to the south. At longitudes corresponding to the Pacific basin, these high-latitude features can be clearly distinguished from the polar frontal zone in the midlatitudes, and collectively resemble the separate Arctic frontal zone discussed by Reed and Kunkel (1960) and Krebs and Barry (1970).

While some separation between high-latitude and

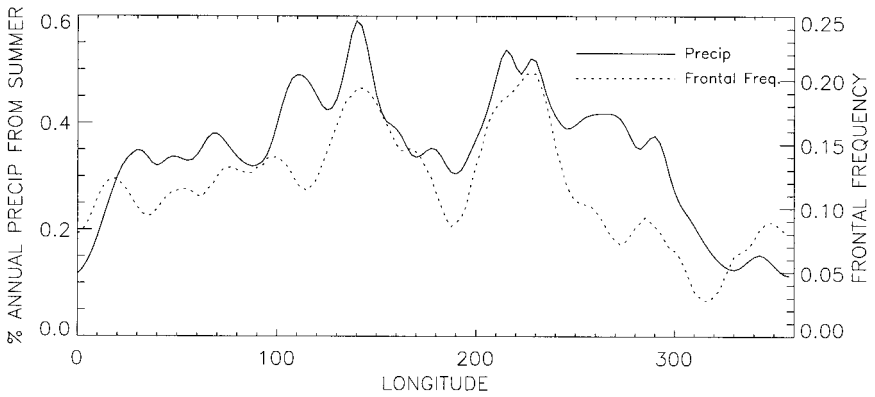

FIG. 13. Longitudinal distribution of summer frontal frequency (fronts day^{-1}) and the fraction of annual precipitation falling in summer, averaged from 62.5° to 67.5°N.

midlatitude frontal activity is apparent in all seasons, the uniqueness of the summer frontal zone is evident from vertical cross sections revealing the existence of deep baroclinicity and associated wind maxima in the upper troposphere. Lending credence to the early view of Dzerdzeevskii (1945), development of the frontal zone is consistent with the effects of strong differential heating between the cold Arctic Ocean and adjacent snow-free land. An association is also found between the regions where frontal activity is best expressed and the presence of significant orography. Clear links are seen between frontal activity, preferred areas of cyclogenesis, and in the longitudinal structure of the contribution of summer precipitation to the annual total.

An initial motivation for the present study was to examine the extent to which the summer Arctic frontal zone may bear on Arctic sea ice variability and the downward trend in ice extent observed in the satellite record (1979–present). From the late 1980s through the mid 1990s, reductions were very pronounced along the Siberian coast during summer and early autumn, associated with increased cyclone activity over the Arctic Ocean promoting offshore winds that enhance melt and advect sea ice away from the coast (Maslanik et al. 1996). We can confirm that cyclones generated in association with the Eurasian frontal zone often track into the central Arctic Ocean. However, as discussed earlier, no trends in the strength of the frontal zone are evident to account for the sea ice reductions and corresponding increases in Arctic Ocean cyclone activity.

At least four studies have argued that the location of the summer Arctic frontal zone may be in part determined by discontinuities in energy exchange and resultant thermal contrasts along the tundra/boreal forest boundary (Hare 1968; Hare and Ritchie 1972; Pielke and Vidale 1996, Pielke et al. 1996). While a vegetation forcing cannot be discounted, our conceptual model does not require it. However, we stress that the low-resolution reanalysis data could mask such associations. A future paper will address the possible role of vegetation along with the effects of coastal baroclinicity and topography from sensitivity studies using the ARCSyM regional model (Lynch et al. 1995).

Acknowledgments. This study was supported by the National Science Foundation under Arctic System Science program Grants OPP-9732461, OPP-9614297, OPP-9910315 and NASA Grant NAG5-6820. We thank R. Barry for helpful comments and R. Kistler for discussions regarding the reanalysis model. The anonymous reviewers are thanked for their constructive efforts.

REFERENCES

Anderson, R., B. Bolville, and D E. McClellan, 1955: An operational frontal contour analysis model. *Quart. J. Roy. Meteor. Soc.,* **81,** 588–599.

Armstrong, R. L., and M. J. Brodzik, 1995: An earth-gridded SSM/I data set for cryospheric studies and global change monitoring. *Adv. Space Res.,* **16,** 155–163.

Barry, R. G., 1967: Seasonal location of the Arctic front over North America. *Geogr. Bull.,* **9,** 79–95.

Blender, R., and M. Schubert, 2000: Cyclone tracking in different spatial and temporal resolutions. *Mon. Wea. Rev.,* **128,** 377–384.

Bolville, B. W., M. A. MacFarlane, and H. A. Steiner, 1959: *An Atlas of Stratospheric Circulation, October 1958–March 1959.* Arctic Meteorology Research Group, McGill University, Defense Research Board, Department of National Defense, Canada, 114 pp.

Bonan, G. B., D. Pollard, and S. L. Thompson, 1992: Effects of boreal forest vegetation on global climate. *Nature,* **359,** 716–718.

——, F. S. Chapin III, and S. L. Thompson, 1995: Boreal forest and tundra ecosystems as components of the climate system. *Climatic Change,* **29,** 145–167.

Bryson, R. A., 1966: Air masses, stream lines, and the boreal forest. *Geogr. Bull.,* **8,** 228–269.

Clarke, L. C., and R. J. Renard, 1966: The U.S. Navy numerical frontal analysis scheme: Further development and a limited evaluation. *J. Appl. Meteor.,* **5,** 764–777.

Colony, R. L., and I. G. Rigor, 1993: International Arctic Ocean Buoy Program data report for 1 January 1992–31 December 1992. Tech. Memo. APL-UW TM 29-93, APL, University of Washington, Seattle, WA, 215 pp. [Available from Applied Physics Laboratory, University of Washington, 1013 NE 40th St., Seattle, WA 98105-6698.]

Defant, F., and H. Taba, 1957: The threefold structure of the atmosphere and the characteristics of the tropopause. *Tellus,* **9,** 259–274.

Dzerdzeevskii, B. L., 1945: Tsirkuliatsionnye skhemy v troposfere Tsentral' noi Arktiki. *Izdatel' svo Akad. Nauk,* 28 pp. (English translation in Scientific Rep. 3 under Contract AF 19(122)-3228 to Dept. of Meteorology, University of California, Los Angeles.)

Foley, J. A., J. E. Kutzbach, M. T. Coe, and S. Levis, 1994: Feedbacks between climate and boreal forests during the Holocene epoch. *Nature,* **371,** 52–54.

Hare, F. K., 1968: The Arctic. *Quart. J. Roy. Meteor. Soc.,* **94,** 439–459.

——, and J. C. Ritchie, 1972: The boreal microclimates. *Geogr. Rev.,* **62,** 333–365.

Hewson, T. D., 1998: Objective fronts. *Meteor. Appl.,* **5,** 37–63.

Huber-Pock, F., and C. Kress, 1989: An operational model of objective frontal analysis based on ECMWF products. *Meteor. Atmos. Phys.,* **40,** 170–180.

Japan Meteorological Agency, 1988: On the improvement of the significant weather chart. *Wea. Serv. Bull.,* **55,** 1–16.

Kalnay, E., and Coauthors, 1996: The NCEP/NCAR 40-Year Reanalysis Project. *Bull. Amer. Meteor. Soc.,* **77,** 437–471.

Krebs, S. J., and R. G. Barry, 1970: The Arctic front and the tundra-taiga boundary in Eurasia. *Geogr. Rev.,* **60,** 548–554.

Kurashima, A., 1968: Studies on the summer and winter monsoons in east Asia based on dynamic concept. *Geogr. Mag. (Tokyo),* **34,** 145–236.

Legates, D., and C. Willmott, 1990: Mean seasonal and spatial variability in gauge-corrected global precipitation. *Int. J. Climatol.,* **10,** 110–127.

Lynch, A. H., W. L. Chapman, J. E. Walsh, and G. Weller, 1995: Development of a regional climate model of the western Arctic. *J. Climate,* **8,** 1555–1570.

——, G. B. Bonan, F. S. Chapin III, and W. Wu, 1999: The impact of tundra ecosystems on the surface energy budget and climate of Alaska. *J. Geophys. Res.,* **104** (D6), 6647–6660.

Maslanik, J. A., M. C. Serreze, and R. G. Barry, 1996: Recent decreases in Arctic sea ice cover and linkages to atmospheric circulation anomalies. *Geophys. Res. Lett.,* **23,** 1677–1680.

McInnes, K. L., J. J. McBride, and L. M. Leslie, 1994: Cold fronts over southeastern Australia: Their representation in an operational numerical weather prediction model. *Wea. Forecasting,* **9,** 384–409.

Palmén, E., 1951: The role of atmospheric disturbances in the general circulation. *Quart. J. Roy. Meteor. Soc.,* **77,** 337–354.

——, and C. W. Newton, 1969: *Atmospheric Circulation Systems. Their Structure and Physical Interpretation.* Academic Press, 603 pp.

Penner, C. M., 1955: A three-front model for synoptic analyses. *Quart. J. Roy. Meteor. Soc.,* **81,** 89–91.

Pielke, R. A., and P. L. Vidale, 1996: The boreal forest and the polar front. *J. Geophys. Res.,* **100,** 25 755–25 758.

——, ——, J. I. Eastman, and A. Barr, 1996: The boreal forest–tundra contrast influence on weather. Preprints, *22d Conf. on Agricultural and Forest Meteorology with Symp. on Fire and Forest Meteorology,* Atlanta, GA, Amer. Meteor. Soc., 98–101.

Reed, R. J., and B. A. Kunkel, 1960: The Arctic circulation in summer. *J. Meteor.,* **17,** 489–506.

Serreze, M. C., 1995: Climatological aspects of cyclone development and decay in the Arctic. *Atmos.–Ocean,* **33,** 1–23.

——, and R. G. Barry, 1988: Synoptic activity in the Arctic Basin. *J. Climate,* **1,** 1276–1295.

——, and C. M. Hurst, 2000: Representation of mean Arctic precipitation from NCEP–NCAR and ERA reanalyses. *J. Climate,* **13,** 182–201.

——, R. G. Barry, and A. S. McLaren, 1989: Seasonal variations in sea ice cover and effects on sea ice concentration in the Canada Basin. *J. Geophys. Res.,* **94,** 10 955–10 970.

——, ——, and J. E. Walsh, 1995: Atmospheric water vapor characteristics at 70°N. *J. Climate,* **8,** 719–731.

——, F. Carse, R. G. Barry, and J. C. Rogers, 1997: Icelandic low cyclone activity: Climatological features, linkages with the NAO, and relationships with recent changes in the Northern Hemisphere circulation. *J. Climate,* **10,** 453–464.

Shapiro, M. A., 1985: Dropwinsonde observations of an Icelandic low and a Greenland mountain-lee wave. *Mon. Wea. Rev.,* **113,** 680–683.

——, R. C. Schnell, F. P. Parungo, S. J. Oldmans, and B. A. Bodhaine, 1984: El Chichon volcanic debris in an Arctic tropopause fold. *Geophys. Res. Lett.,* **11,** 421–424.

——, T. Hampel, and A. J. Krueger, 1987: The Arctic tropopause fold. *Mon. Wea. Rev.,* **115,** 444–454.

Whittaker, L. M., and L. H. Horn, 1984: Northern Hemisphere extratropical cyclone activity for four mid-season months. *J. Climatol.,* **4,** 297–310.

Willis, R. A., and G. K. Grice, 1977: The wintertime Arctic front and its effect on Fairbanks, Alaska. *Mon. Wea. Rev.,* **105,** 78–85.

Yoshimura, M., 1967: Annual change in frontal zones in the Northern Hemisphere. *Geogr. Rev. Japan,* **40,** 393–408.

Zwatz-Meise, V., and G. Mahringer, 1988: Use of satellite imagery, combined with numerical model diagnostics, to locate fronts and predict their activity: Methods and examples. *Satellite and Radar Imagery Interpretation, Preprints for a Workshop in Reading, England, 20–24 July 1987,* M. Bader and T. Waters, Eds., Eumetsat, 143–162.